

Light Harvesting by Chlorophylls and Carotenoids in the Photosystem I Core Complex of *Synechococcus elongatus*: A Fluorescence Upconversion Study

John T. M. Kennis,[†] Bas Gobets,[‡] Ivo H. M. van Stokkum,[‡] Jan P. Dekker,[‡]
Rienk van Grondelle,[‡] and Graham R. Fleming^{*,†}

Department of Chemistry, University of California, and Physical Biosciences Division, Lawrence Berkeley National Laboratory, Berkeley, California 94720, and Department of Biophysics and Physics of Complex Systems, Faculty of Sciences, Vrije Universiteit, De Boelelaan 1081, 1081 HV Amsterdam, The Netherlands

Received: January 31, 2001

The photosystem I (PSI) core complex of oxygenic photosynthesis is an integral pigment–protein complex that incorporates both the antenna and the reaction center (RC). It binds about 100 Chl *a* and 20 β -carotene molecules. In the PSI core complex of the cyanobacterium *Synechococcus elongatus*, a total of about 9 antenna Chl *a* molecules are red-shifted with respect to the primary electron donor, which absorbs at 700 nm. We have studied energy transfer and trapping processes in trimeric PSI complexes of this species at femtosecond resolution by means of the fluorescence-upconversion technique. By simultaneously analyzing the fluorescence upconversion results and those obtained with a streak camera with picosecond resolution and multichannel detection (Gobets, B.; et al. *Biophys. J.*, in press), we have mapped out the energy transfer processes that follow immediately after photon absorption. Equilibration among Chl *a* pigments in the bulk antenna was found to occur with a time constant of 360 fs. A major energy equilibration phase between bulk Chl *a* and the red-shifted antenna Chls occurs in 3.6 ps. A slow phase in energy equilibration takes place in 9.8 ps, after which the excitations are trapped by the RC in 38 ps. Fluorescence anisotropy measurements indicated an initial anisotropy of 0.30, which decayed biphasically with a major fast phase of 160 fs and a minor slow phase of 1.8 ps to a final anisotropy of 0.06. The 160 fs phase is assigned to elementary energy transfer steps in the bulk Chl *a* antenna, and the 1.8 ps phase to further equilibration processes, possibly involving energy transfer to or among red-shifted Chls. Energy transfer from β -carotene to Chl *a* was found to proceed both from the S₂ state and the S₁ state, with the majority of transferred excitations (60%) originating from the S₂ state, resulting in an estimated overall yield of ~90%. A comparison is made with the PSII core antenna protein CP47, which binds the same pigments but has a substantially lower carotenoid–Chl *a* energy transfer yield of ~35% (van Dorssen R. J.; et al. *Biochim. Biophys. Acta* **1987**, 893, 267).

Introduction

The core complex of photosystem 1 (PSI) of oxygenic photosynthesis is a large, multisubunit integral membrane pigment–protein complex that uses light energy to catalyze electron transfer from cytochrome *c*₆ or plastocyanin to NADP⁺. It binds about 100 chlorophyll (Chl) *a* and 20 β -carotene molecules¹ and, in that sense, forms the largest and most complex known photosynthetic energy converting protein. A 4 Å structure of the PSI core complex of the cyanobacterium *Synechococcus elongatus* in its trimeric form has been available for some years now.^{1,2} Each monomeric unit in the trimeric structure comprises 11 subunits termed PsaA through PsaF and PsaI through PsaM. PsaA and PsaB are the largest and most important subunits and are arranged in a pseudo-C₂ symmetry at the center of the complex. PsaI, PsaL, and PsaM lie at the periphery of the core complex near the trimerization domain. A total of 89 Chl *a* molecules were resolved in the entire complex. At the center, 6 Chls are bound to PsaA and PsaB close to the pseudo-C₂ axis and were assigned as the redox active chromophores of the reaction center (RC). They are arranged

in a fashion that is reminiscent of the purple bacterial RC, with two Chl *a*'s as a special pair, two “monomeric” Chl *a*, and two Chl *a*'s at the position of the bacteriopeophytins.¹

The other 83 Chl *a* molecules resolved in the complex constitute the PSI core's light harvesting system. A majority of 77 of them are bound to PsaA and PsaB. The core antenna Chls form an ellipsoidically shaped, irregular bowl around the reaction center at distances ranging between 15 and 40 Å. The Chl *a* molecules in the core antenna are densely packed at distances from 8 to 16 Å. The 4 Å structure resolution did not allow for an identification of any of the about 20 β -carotene molecules.

A conspicuous feature of the light-harvesting system of cyanobacterial PSI in general is the presence of several Chl *a* molecules that have their excited state energies red-shifted significantly below that of the primary donor (P700) of the RC. In the PSI core, the number of red Chls and the extent of red-shifting depend on the species and the aggregation state (monomeric or trimeric) of the complex. A pool that absorbs maximally at 708 nm at low temperature (4 K), hereafter referred to as C708, appears to be a common feature to all cyanobacterial PSI core particles. It was proposed some years ago that, in the cyanobacterium *Synechocystis* PCC6803, C708 corresponds to the lower excitonic state of a strongly coupled dimer or trimer

* Corresponding author. Telephone: 510-643-2735. E-mail: GRFleming@lbl.gov.

[†] University of California and Lawrence Berkeley National Laboratory.

[‡] Vrije Universiteit.

of Chl *a* molecules.³ Studies on a series of mutants of *Synechocystis*, which each had one of their peripheral subunits deleted, indicated that C708 is most likely bound to the periphery of PsaA and/or PsaB, near the L and M subunits.^{4,5} Some species have an additional red pool which absorbs more to the red than C708. These generally suffer loss of absorption upon monomerization of the complexes, which suggests that they are located at the periphery of the core complex near the trimerization domain.⁶

The function of the red pigments is a matter of considerable debate. In fact, the presence of different pools in the various species may indicate that they have different functions. It has been suggested that they could increase the efficiency of energy trapping by concentrating excitations near the RC.^{7,8} However, this is contradicted by recent experiments which demonstrated that PSI preparations with a progressively increasing number of red Chls exhibit increasing lifetimes in the core antenna.⁹ A more likely explanation would be that the absorption cross section of far red light is increased by the presence of the red pigments,¹⁰ which in the case of considerable shading of leaves or cyanobacterial mats may significantly increase the photochemical turnover rate.¹¹ Alternatively, the red Chls may be involved in photoprotective mechanisms.¹²

PSI core particles bind about 20 β -carotene molecules per monomer, which give rise to a broad absorption band in the blue and green parts of the solar spectrum. They are the only PSI core pigments that absorb significantly in that wavelength region, which may imply an important role for β -carotene as accessory light harvesting pigments. We remark that cyanobacteria employ phycobilisomes, which are extramembrane light harvesting complexes, to fill the spectral gaps left open by Chl *a*. These complexes absorb yellow and orange and in some cases blue-green light, but under most circumstances they transfer their excited state energy primarily to PSII.¹³

The light-harvesting function of β -carotene in the PSI core is exemplified by the high energy transfer efficiency to Chl *a* of about 85%.¹⁴ Such a high efficiency, often seen in photosynthetic systems, is remarkable in the light of the short lifetime of carotenoid excited states. The optically allowed S_2 state of carotenoids generally relaxes to the optically forbidden S_1 state in 100–200 fs by internal conversion (IC), after which the S_1 state internally converts to the ground state on a picosecond time scale.^{15,16} For an efficient light harvesting function of carotenoids, these IC processes must be counteracted by faster energy transfer to Chl. Indeed, it has recently been shown that in photosynthetic antennae, subpicosecond and picosecond energy transfer from both the S_2 and S_1 state to (B)Chl can effectively compete with IC to the ground state.^{17–22}

Energy transfer and trapping processes in the PSI core have been studied quite extensively by time-resolved absorption and fluorescence techniques for many years now^{7,23–26} (for a review of early work see ref 8). Only recently, however, the time resolution and sensitivity of the measuring equipment have come to a point that all relevant energy transfer steps can be mapped out in an annihilation-free regime. Low-energy transient absorption studies with femtosecond time resolution have focused on PSI cores of the cyanobacterium *Synechocystis* PCC6803.^{27–29} Recent time-resolved fluorescence measurements with ps resolution utilizing a streak camera with multiwavelength detection have compared the excited-state dynamics of PSI cores of several cyanobacterial species.^{9,30,31} All this research has exclusively addressed Chl *a* dynamics, and thus far, the light-harvesting process that involves energy transfer from β -carotene to Chl *a* has remained uninvestigated.

In this paper we present a fluorescence upconversion study on trimeric PSI particles of the cyanobacterium *Synechococcus elongatus*. The trimeric PSI core of this species contains two pools of red Chls, the common pool C708 and an additional pool C719 after its absorption maximum at low temperature.^{32,33} By combining spectrally resolved upconversion data with femtosecond resolution with those obtained by means of a multichannel streak camera, we have mapped out energy equilibration components between bulk Chl *a* molecules, between bulk Chl *a* and the red pools, and subsequent trapping by the RC. Furthermore, we present time-resolved fluorescence anisotropy measurements, which indicate the time scale of elementary energy transfer steps in the PSI core antenna. Finally, we have characterized the dynamic aspects of the energy transfer process from β -carotene to Chl *a*.

Experimental Section

Trimeric complexes from the cyanobacterium *Synechococcus elongatus* were prepared as described previously.³⁴ For the fluorescence measurements, the concentrated samples were diluted to an absorbance at 680 nm of 0.3/mm with a buffer containing 20 mM CaCl₂, 20 mM MgCl₂, 10 mM 2-(*N*-morpholino)ethanesulfonic acid (MES), and 0.05% w/v dodecyl- β -D-maltoside at a pH of 6.5. Although we were working with closed (oxidized) RCs (see below), 10 mM sodium ascorbate and 10 μ M phenazine metasulfate (PMS) were added to the samples. We found that addition of these chemicals slowed photodegradation of the sample during the measurements by a factor of at least 3, enabling us to utilize longer data collection times. The sample was flowed through a 1 mm path length quartz cell using a peristaltic pump and maintained at 8–10 °C by a recirculating bath that flowed around the sample reservoir. The sample was exchanged for a fresh one every \sim 3 h of data collection. The absorption spectra of the used samples revealed no significant degradation.

Fluorescence upconversion measurements were carried out with an apparatus described previously.¹⁹ At its basis was a regeneratively amplified Ti:sapphire laser system (Coherent Mira-Rega), operating at 250 kHz with a pulse duration of about 50 fs. Excitation pulses at 400 nm were provided by frequency doubling the output of the laser system in a 2 mm long BBO crystal. Excitation pulses at 650 or 510 nm were generated by means of an optical parametric amplifier (OPA, Coherent 9450). The instrument response function of the upconversion apparatus ranged between 280 and 350 fs. The polarization of the excitation beam with respect to the polarization of the upconverted fluorescence was set to either parallel, perpendicular, or at the magic angle (54.7°) by means of an achromatic waveplate (CVI). For fluorescence anisotropy measurements, the polarization was alternately switched between parallel and perpendicular many times to avoid any possible effect of long-term fluctuations in the laser and detection system or sample conditions. A test measurement of the anisotropy in the dye LDS 720 upon excitation at 650 and detection at 725 nm gave a nondecaying anisotropy of 0.36, which is close to the expected value of 0.4.

Initially, it was our goal to perform the measurements with P_{700} in the open (reduced) state. However, we found that this would require unattainable low excitation powers. To achieve reasonable count rates (\sim 40 counts/s) necessary for efficient data collection, we had to employ 2 mW of excitation energy, corresponding to a pulse energy of 8 nJ. At such pulse energies and with estimation of a focal diameter of 100 μ m, we expect that about 1 out of 100 Chls is excited in the focal volume,

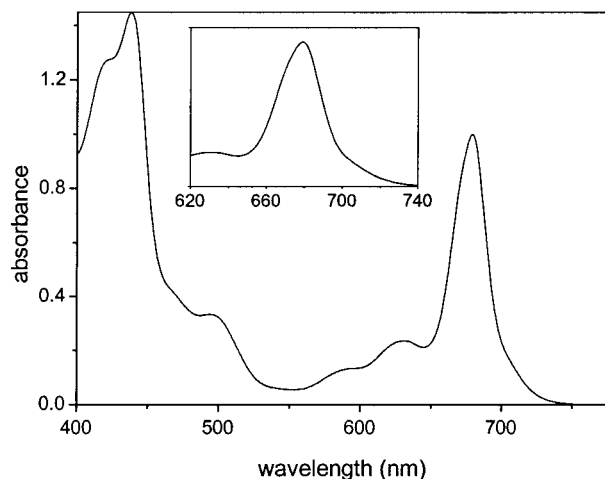


Figure 1. Absorption spectrum of trimeric PSI particles of *Synechococcus elongatus* at room temperature. The inset shows the Chl *a* Q_y absorption region on an expanded scale.

which corresponds to about 1 Chl in every PSI monomer, and thus all RCs are oxidized after the sample in the excited volume has received a few shots. Given a 250 kHz repetition rate of the laser system and a flow speed of 0.5 m/s, a given volume of PSI particles resides 0.2 ms in the focus and is exposed to about 50 laser shots while moving through. During this time, P_{700}^+ is not reduced by the combination of sodium ascorbate and PMS, as this process takes place on a millisecond time scale.³⁵ Hence, these circumstances will lead to a vast majority of >90% oxidized RCs in the excited volume.

The above estimate of the excitation density indicates that we are near the threshold for singlet–singlet annihilation. To test for annihilation effects, the excitation power was varied between 0.3 and 3 mW. This did not alter the upconverted trace (data not shown), from which we conclude that we were measuring in a regime where singlet–singlet annihilation does not play a significant role. We note that our pulse energies are below those given by Savikhin et al. for the onset of annihilation.²⁷ Singlet–triplet annihilation is unlikely to arise given the low triplet yield of Chl *a* in the PSI core (by virtue of the short Chl *a* antenna lifetime of ~ 40 ps). Moreover, any Chl *a* triplet will likely be rapidly quenched by β -carotene.

Some of the time-resolved data were analyzed with a global fitting program as described in ref 36. Species-associated spectra (SAS) were determined assuming a sequential, irreversible model $A \rightarrow B \rightarrow C \rightarrow D$. The arrows symbolize increasingly slower monoexponential decays, with time constants that can be regarded as the species lifetimes. This procedure enables us to visualize clearly the evolution of the excited states in the system. Note, however, that the thus obtained species A–D are not necessarily pure but may represent mixtures of pure states. The anisotropy measurements were analyzed following the method of Cross and Fleming by simultaneously fitting the polarized and magic angle traces with sums of exponential functions, convoluted with the instrument response function.³⁷

Results and Discussion

Figure 1 shows the absorption spectrum of trimeric PSI particles of *Synechococcus elongatus* at room temperature. The absorption features at wavelengths longer than 600 nm result exclusively from the Q_y transition of Chl *a* and are shown on an expanded scale in the inset. The absorption band with a maximum at 680 nm is associated with bulk Chl *a* pigments in the core antenna. This band is markedly asymmetric and shows

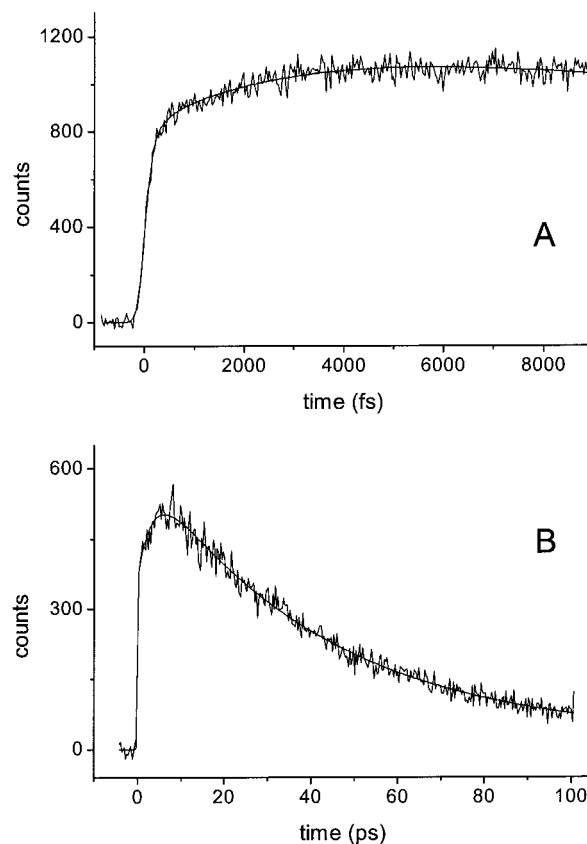


Figure 2. (A) Time-resolved isotropic fluorescence in trimeric *Synechococcus elongatus* PSI particles, detected at 725 nm upon excitation at 650 nm, collected on a time basis of 9 ps. (B) Time-resolved trace collected under the same conditions as (A), on a time basis of 100 ps. The traces are fitted with a 4-component exponential function with time constants of 210 fs, 3.3 ps, 41 ps, and a long-lived end level with relative amplitudes $-0.18:-0.39:1:0.04$. See text for details.

a shoulder near 670 nm, indicating significant spectral heterogeneity among bulk antenna Chls. Near 630 nm a vibronic band of Chl *a* is located. At wavelengths longer than 700 nm the spectrum shows a distinct long tail, which is due to the two pools of red-shifted Chls, C708 and C719. These two pools contain 4–5 and 4 Chls, respectively.³² It is important to note that, at room temperature, the absorption maxima of C708 and C719 are probably located at 702 and 708 nm, respectively.^{4,9} In the blue region, the absorption spectrum shows a maximum at 440 nm, which can be assigned to the Soret band of Chl *a*. The absorption band near 500 nm is associated with β -carotene, of which about 20 molecules are bound per PSI monomer. All absorption features shown in Figure 1 are similar to those published earlier for this preparation.^{32,33}

The room-temperature steady-state fluorescence spectrum of *Synechococcus* trimers was published previously.³³ It shows a maximum at 720 nm, which can primarily be attributed to fluorescence from the red pools C708 and C719, and a pronounced shoulder at 690 nm, which originates from bulk Chl *a* in thermal equilibrium with the red pools.

Isotropic Time-Resolved Fluorescence. We characterized energy transfer processes between bulk Chl *a*, the red pools C708 and C719, and the RC by performing fluorescence upconversion measurements with excitation in the vibronic band of bulk Chl *a* at 650 nm and detection at 725 nm, where we primarily observe fluorescence from the two pools of red pigments, C708 and C719, which contribute roughly equally here.⁹ Figure 2 shows the upconverted fluorescence detected at

the magic angle in *Synechococcus* trimers with closed RCs on a short (A) and long time axis (B), respectively. Several distinct time scales ranging from instantaneous to tens of picoseconds can be discerned in this measurement. A simultaneous fit to the traces yields an instantaneous component, a rise time of 210 fs with a minor amplitude, a major rise time of 3.3 ps, a decay component time of 41 ps, and a minor long-lived end level.

The instantaneous component can be assigned to emission from the directly excited bulk Chl *a* molecules, which have a significant vibronic tail at this wavelength.⁹ The amplitude of the 210 fs rise component is small (18% with respect to the overall 41 ps decay component), and from this measurement alone we cannot deduce its origin. The 3.3 ps rise time can readily be ascribed to energy equilibration between bulk Chl *a* and the red pools C708 and C719. It closely matches the value of 3.8 ps that has been determined before on the same species by means of a streak camera with ps resolution.⁹ It is significantly shorter than the equilibration times of 7 ps reported by Holzwarth et al.⁷ and 13 ps by Byrdin et al.³⁵ for *Synechococcus* trimers, but the determination of these values were severely hampered by the limited time resolution of both experiments. The 3.3 ps equilibration time is similar to the corresponding time constants reported recently with fs transient absorption spectroscopy for PSI particles of *Synechocystis PCC6803*.^{27,29}

The 41 ps component can be assigned to excitation quenching by the oxidized RCs. It agrees well with the lifetime of 37 ps which has been reported in recent photon counting measurements on closed RCs in *Synechococcus* trimers by Byrdin et al.³⁵ and is virtually indistinguishable from that reported for open RCs in this species.^{7,9,35} The lifetime of 41 ps is significantly longer than that found in plant PSI cores (22 ps) (B. Gobets, unpublished results) and the PSI core of *Synechocystis* (25 ps).^{9,26,30,31} Gobets et al. have recently shown that an increasing number of red Chls leads to longer trapping times, as is the case with *Synechococcus*. The species with the highest red Chl content known to date, *Spirulina platensis*, has a lifetime of 50 ps.⁹ The long-lived component has minor amplitude (4%) and can be attributed to a small fraction of unbound Chl *a*, which has a lifetime in the order of 5 ns.

To obtain a more complete picture of excited-state equilibration in the core antenna of *Synechococcus*, we performed fluorescence upconversion experiments with excitation in the Chl *a* Soret band at 400 nm and detection at 8 different wavelengths from 668 to 738 nm, which covers the fluorescence emitted from all spectral forms in the PSI core. It would have been desirable to perform these wavelength-resolved measurements with direct excitation in the Q_y band, but as a result of strong scattering by the pump beam at 650 nm, it was not possible to upconvert the fluorescence at wavelengths shorter than about 710 nm. With excitation in the Soret band, all Chl *a* molecules, including the red pigments, have an equal excitation probability, and they will relax to the Q_y state in ca. 100 fs.³⁸ Figure 3 shows four selected traces at 668 nm, 687, 705, and 727 nm.

The trace at 727 nm, which monitors fluorescence from the red pools C708 and C719, is very similar to the trace presented in Figure 2A upon excitation at 650 nm and detection at 725 nm. It exhibits a rapid rise of the fluorescence, which mainly represents bulk Chl *a* fluorescence following relaxation from the Soret to the Q_y state. It then rises further on a time scale of a few picoseconds, indicating equilibration between the bulk and the red pigments. Correspondingly, the traces at 668, 687,

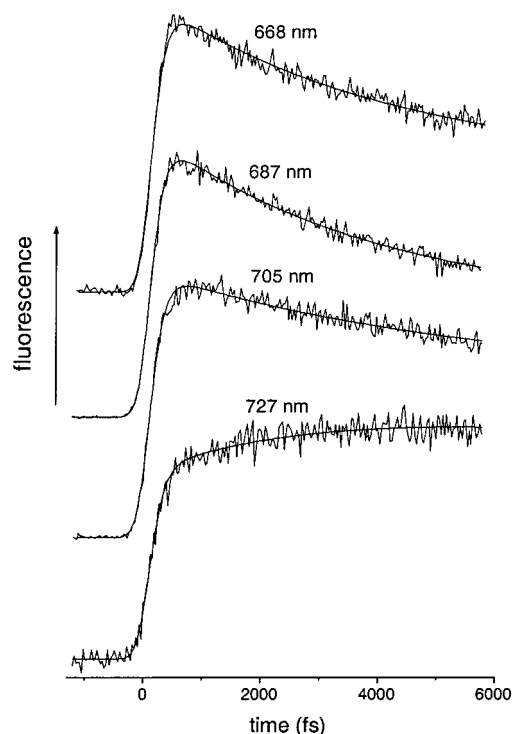


Figure 3. Time-resolved isotropic fluorescence in trimeric *Synechococcus elongatus* PSI particles upon excitation at 400 nm, detected at 668 nm, 687, 705, and 727 nm. The traces are fitted with triexponential functions with time constants of 140 fs, 3.3 ps, and 41 ps (see text for details).

and 705 nm, which probe fluorescence from bulk Chl *a*, display a decay on a picosecond time scale. All traces are fitted well with the time constants of 3.3 ps (with positive amplitude at 668, 687, and 705 nm and negative amplitude at 727 nm) and 41 ps found in the measurement presented in Figure 2.

Close inspection of the early time behavior of the traces in Figure 3 indicates that the rise of the fluorescence at 705 nm lags that of the trace at 668 nm by a few hundreds of femtoseconds. To demonstrate this, we fitted the traces with a single rise time of 140 fs, assuming that the sample does not fluoresce at time zero. In principle, 140 fs is not an unreasonable number for Soret- Q_y relaxation. However, at 668 nm the fit undershoots the experimental data at early times, while at 705 nm the fit overshoots the data. If we assume that Soret- Q_y relaxation takes place at a uniform, wavelength-independent rate, this indicates that an additional subpicosecond dynamic process is taking place in the PSI core antenna. Because the lag in the rise occurs at the red side of the bulk Chl *a* fluorescence (and not at a wavelength where fluorescence from the red pigments dominates, as evidenced by the positive 3.3 ps component at 705 nm; see also ref 9), we assign this component to a dynamic process taking place in bulk Chl *a* molecules. We will substantiate this point below.

For a meaningful characterization of the time-dependent fluorescence behavior in the PSI core antenna, it is highly desirable to apply a global analysis of the spectrally resolved time-dependent traces and determine the relative intensities across the fluorescence spectrum, in the form of so-called species-associated spectra. However, with the fluorescence upconversion technique, a quantitative determination of the relative fluorescence intensities at different detection wavelengths is cumbersome, which means that the construction of time-resolved or species-associated spectra cannot be reliably conducted. We have noted already the consistency of the present

fluorescence upconversion data and the wavelength-resolved streak camera data reported earlier,⁹ which encouraged us to perform a simultaneous global analysis of these two data sets. This approach allows us to maximally utilize the spectral and temporal information that is provided by our measurements and follow the spectrally resolved dynamics from ~ 100 fs after photon absorption to more than 100 ps, after which all excited states have been trapped by the RC. In this analysis, the early dynamics up to about 1.5 ps are mainly extracted from the fluorescence upconversion measurements. The dynamics between 1.5 and 6 ps are extracted from both datasets, and the dynamics slower than 6 ps are obtained exclusively from the streak camera data. In essence, the overlapping time ranges of both experiments allow us to assign a spectral evolution to the early time window.

We forewarn the reader that the experimental circumstances under which the two datasets were collected were not identical. The largest difference is that the upconversion data were collected with oxidized RCs and the streak camera data with reduced RCs. However, thus far all reports dealing with open and closed RCs on PSI particles have indicated a very similar evolution in these two cases.^{28,35} The analysis of the streak camera data was published earlier and indicated that five lifetimes are necessary to describe the data: 400 fs; 3.8 ps; 9.6 ps; 38 ps; 3 ns.⁹ It is important to note that, in this case, the 400 fs component was limited by the instrument response and represented a rise of fluorescence, which was ascribed to Chl *a* Soret– Q_y relaxation.

In the new, simultaneous analysis it was assumed that no fluorescence originates from the sample at time zero and rises with the Soret– Q_y relaxation time. This relaxation time can be estimated to be 100 fs,³⁸ which is significantly shorter than that estimated in the earlier analysis of the streak camera data.⁹ We found that 6 components are required for an adequate description of the complete dataset. Figure 4 shows the upconversion traces plotted together with the streak camera traces, along with the results of the global analysis. Note that the time axis is linear from -2 to 5.8 ps and logarithmic at longer times. Strikingly, the upconversion traces connect smoothly to the streak camera traces. The time constants that follow from the simultaneous global analysis are 100 fs, 360 fs, 3.6 ps, 9.6 ps, 38 ps, and 3 ns. The species-associated spectra (SAS) that follow from this analysis are shown in Figure 5. Note that, to obtain these SAS, we have assumed a sequential model in which the first SAS decays into the second SAS, etc. (see Experimental Section). The SAS with a lifetime of 100 fs represents the Soret state of Chl *a*, which we require to be zero in this wavelength region and is not shown.

The first displayed SAS (squares) rises in 100 fs and has a lifetime of 360 fs. It peaks at about 687 nm and can thus be assigned to fluorescence emanating primarily from bulk Chl *a* pigments. The next SAS (solid circles), which is formed in 360 fs, has a lifetime of 3.6 ps. It is slightly red-shifted with respect to the former SAS by a few nanometers. The extent of the red-shift cannot be accurately determined because of the coarse wavelength intervals used. The wavelengths associated with this red shift can be attributed to fluorescence changes that originate from the bulk of the PSI core antenna and not the red pools C708 and C719. We accordingly assert that the 360 fs component represents excited-state energy equilibration among bulk Chl *a* molecules. Similar time constants, assigned to the same process, were observed using femtosecond pump–probe spectroscopy in PSI particles of *Synechocystis* PCC6803 upon excitation at the blue side of the Q_y band.^{27,29} Our measurements

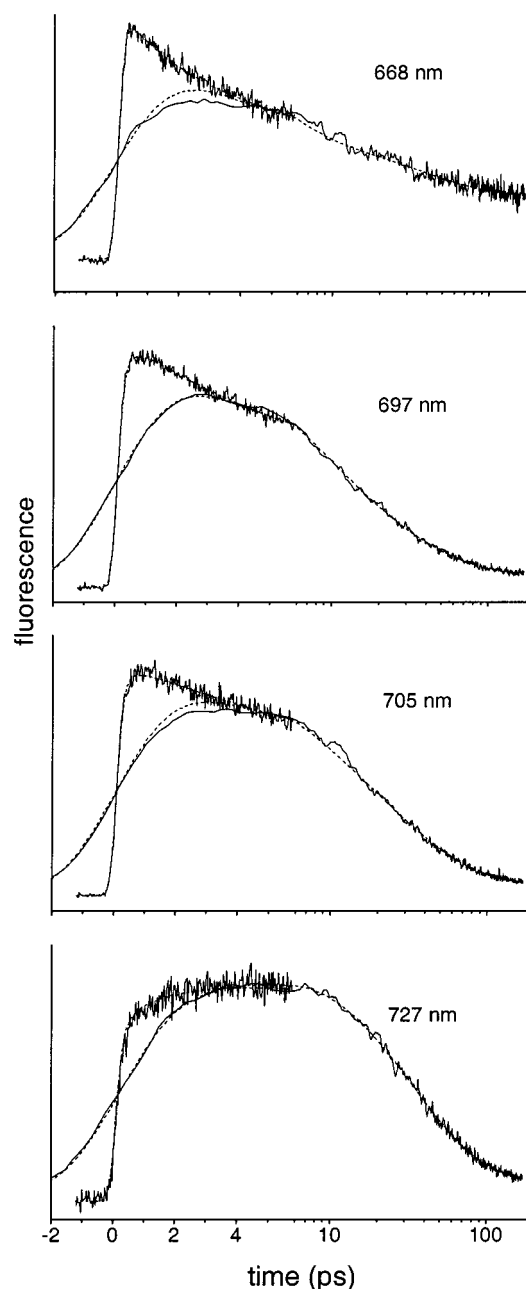


Figure 4. Fluorescence upconversion traces obtained in *Synechococcus elongatus* PSI particles combined with those obtained with a streak camera (solid lines),⁹ plotted on a linear–logarithmic time axis. The dotted lines denote the result of the 6-component simultaneous analysis of the upconversion and streak camera data. The excitation wavelength was 400 nm, and the detection wavelengths (from top to bottom) were 668, 697, 705, and 727 nm. See text for details.

thus form the fluorescence-detected counterpart of these observations and indicate that this process is also discernible upon excitation at 400 nm, which is nonselective and results in a more even initial excited state distribution between the different spectral forms in the core antenna. We note that the 360 fs time constant is similar to the 210 fs rise component that we detected at 725 nm with excitation at 650 nm (Figure 2A). The SAS of Figure 5 (squares vs solid circles) show that the 360 fs component has the same sign and a similar amplitude, which makes it likely that these components have the same origin.

The next SAS (triangles) is formed in 3.6 ps and has a lifetime of 9.8 ps. It represents a large red shift of about 20 nm, having a shallow maximum near 715 nm, and thus implies a drastic shift toward thermal equilibrium in the PSI core antenna. This

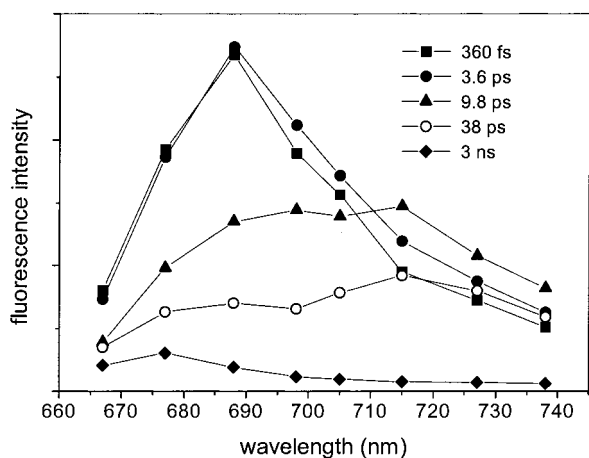


Figure 5. Species-associated spectra (SAS) that follow from the 6-component simultaneous analysis of the isotropic fluorescence upconversion data presented in Figure 4 and streak camera data of ref 9 of trimeric *Synechococcus elongatus* PSI particles.

newly formed fluorescence band is associated with the red pools C708 and C719; therefore, the 3.6 ps process can clearly be assigned to equilibration between the bulk Chl *a* and the red pools C708 and C719. Note that the process appears to be nonconservative; i.e., the area under the 360 fs SAS is larger than that under the 3.6 ps component, indicating that some excited states are quenched. This may indicate that some nonequilibrium energy trapping by the RC occurs, as observed before for some PSI preparations.^{9,30} The 3.6 ps component is the only component in this analysis which adopts weight from both the upconversion and streak camera datasets. The shape of the SAS and the value of the time constant are very similar to what follows from the analysis of the streak camera data alone, which substantiates the consistency of the two datasets.

The longer-lived components all follow from the streak camera data and have been characterized previously.⁹ The next component (open circles) rises in 9.8 ps and has a lifetime of 38 ps. With regard to the previous SADS, it is slightly further red-shifted, along with a significant decrease of fluorescence intensity, which indicates that the 9.8 ps process signals slow energy equilibration with the red pigments and a significant portion of energy transfer to the RC. The 38 ps component represents the transfer-equilibrated state in the core antenna^{9,31} and is exclusively associated with energy transfer to the RC. Its shape is similar to that of the steady-state fluorescence spectrum reported in ref 33. The 3 ns component has a small amplitude and peaks near 675 nm and is caused by a fraction of loose, unbound Chl *a*.

We also performed a simultaneous analysis of these data with 5 components, i.e., 1 component less than in the above analysis. We found that the fit becomes slightly worse, by 2%, and the time constants become 140 fs, 2.5 ps, 7.4 ps, 34 ps, and 5 ns. The only significant difference with the above analysis lies in the subpicosecond time constants; the rest of the components remains qualitatively the same. With 5 components, the Soret– Q_y relaxation time constant is fitted to 140 fs, (see Figure 3), whereas, with 6 components, the subpicosecond times were split in a Soret– Q_y relaxation time of 100 fs and a bulk Chl *a* equilibration component of 360 fs.

Time-Resolved Fluorescence Anisotropy. To further characterize the time scale of elementary energy transfer steps in the PSI antenna, we performed time-resolved fluorescence anisotropy measurements on trimeric PSI particles of *Synechococcus elongatus*. From top to bottom, Figure 6 shows the

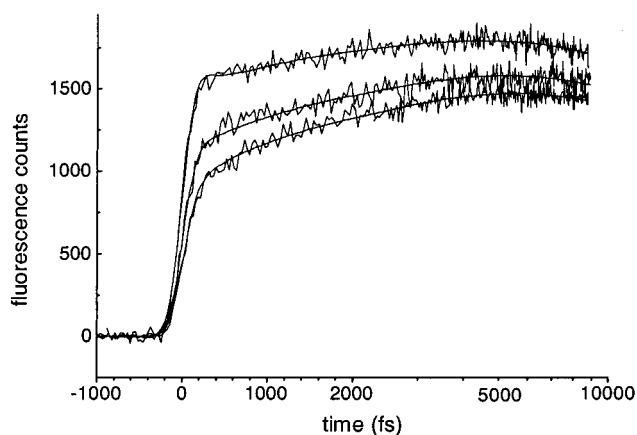


Figure 6. Polarized time-resolved fluorescence of trimeric *Synechococcus elongatus* PSI particles, with from top to bottom, excitation and detected fluorescence polarized parallel, at the magic angle, and perpendicular. The excitation wavelength was 650 nm, and fluorescence was detected at 725 nm. Note that the time scale is linear from –1 to 2 ps and logarithmic from 2 to 8 ps. The smooth solid lines denote the result of an anisotropy analysis, which yielded an anisotropy decay function $r(t) = 0.14 \exp(-t/0.16) + 0.1 \exp(-t/1.8) + 0.06$, with the time constants given in picoseconds.

upconverted fluorescence with excitation and detected fluorescence polarized parallel, at the magic angle, and perpendicular, detected at 725 nm upon excitation at 650 nm. (The magic angle trace is reproduced from Figure 2A). We observe that at early times, especially during the rising part, the trace with parallel polarization has significantly higher intensity than the perpendicular trace, implying a substantial fluorescence anisotropy. Note that although the detection wavelength corresponds to that of the red pigments, the subpicosecond signals are dominated by fluorescence that originates from the vibronic tail of bulk Chl *a* (see above). At increasing delays, the parallel and perpendicular traces move closer together, indicating fluorescence anisotropy decay.

To determine the time-resolved anisotropy $r(t)$, we analyzed these data according to the method of Cross and Fleming by simultaneously fitting the polarized and magic angle traces to a sum of exponential functions, convoluted with the instrument response function.³⁷ In the analysis, we also took into account the long magic angle scan of 100 ps shown in Figure 2B to properly determine the time constants in the isotropic contribution to the signals. The result of this analysis is shown as the smooth solid lines in Figure 6. We find an initial anisotropy $r(0)$ of 0.30, which decays biphasically with time constants of 160 ± 60 fs (amplitude 0.14) and 1.8 ± 0.2 ps (amplitude 0.10) to a final, nondecaying value of 0.06 ± 0.015 . A test measurement on a laser dye in solution gave a time-independent anisotropy of 0.36, which is reasonably close to the theoretically expected value of 0.4 for the initially prepared excited state (see Experimental Section). In the PSI core, we observe an initial anisotropy $r(0)$ of 0.30, which is somewhat lower than the reference measurement, indicating that we do not detect the anisotropy decay of the entire initially prepared Chl *a* ensemble. Fixing the initial anisotropy to 0.36 in the analysis gave a fast anisotropy decay of 95 ± 15 fs (amplitude 0.2), a slow one of 1.6 ± 0.14 ps (amplitude 0.1), and a nondecaying component of 0.06. The quality of the fit was similar to that shown in Figure 6. (Result not shown.)

Our results are very similar to the fluorescence upconversion measurements of Du et al. on PSI particles of *Chlamydomonas reinhardtii*, who reported an initial anisotropy of 0.34 which decayed with a time constant of 180 fs.²³ We note that the

excitation and detection wavelengths in our and Du's studies were similar but that the instrument response function of Du's study was significantly shorter (100 fs vs 280 fs). Savikhin et al. employed polarized femtosecond transient absorption spectroscopy on PSI core particles of *Synechocystis*.²⁷ Upon excitation and probing in bulk Chl *a*, they found an initial anisotropy of 0.27 which decayed monophasically to 0.07 with a time constant of 590 fs, which appears to be at odds with our results. However, Savikhin et al. analyzed their data by determining the raw anisotropy $r_{\text{raw}}(t) \approx (I_{\text{par}} - I_{\text{perp}})/(I_{\text{par}} + 2I_{\text{perp}})$ and subsequently fitting $r_{\text{raw}}(t)$ with a sum of exponentials. As pointed out before, this procedure may lead to considerable errors because it does not take into account the effects of a finite instrument response.³⁷ When we apply a similar procedure to our fluorescence upconversion data and fit the resulting raw anisotropy $r_{\text{raw}}(t)$ with a biexponential function, we also find an initial anisotropy of 0.27, which decays with a major time constant of 560 fs (0.17 amplitude) and a minor one of 6 ps (0.055 amplitude) to a nondecaying value of 0.046. This suggests that it may be the analysis of the time-resolved data and not the experimental data themselves that are the source of the apparent incompatibility of our results and those of Savikhin et al.

A fast anisotropy decay of 160 fs would be consistent with the structural information we have for the PSI core: the close packing of Chls in the PSI core antenna, with center-to-center distances ranging from 7 to 16 Å and an average coordination number of about 3 within this range of distances,¹ is expected to lead to site-to-site hopping times (or perhaps excitonic relaxations) in the order of 100 fs, as has been extensively documented by anisotropy measurements on the LH1 and LH2 complexes of purple bacteria^{39–42} and the FMO complex of green sulfur bacteria,^{43,44} which have comparable interpigment distances. Structure-based simulations of energy transfer and trapping in the PSI core have indicated Chl *a* single-site lifetimes in the order of 100 fs (B.Gobets, manuscript in preparation).

A relatively slow anisotropy decay with an amplitude of 0.1 occurs with a time constant of 1.8 ps. It is not very likely that this component is associated with one specific process; it probably follows from the combined effects of slow energy equilibration in bulk Chl *a*, energy transfer processes between bulk and red Chl *a*, and perhaps equilibration processes among the red pools C708 and C719, which may all have their specific time scales of which 1.8 ps forms some weighted average. The final anisotropy is 0.06, which is close to zero, as one would expect for an orientationally disordered system as PSI. Note that, in the study of Du et al., the final anisotropy did not vanish but remained constant at 0.2 at long delays.²³ This was probably an artifact, possibly caused by the presence of a fraction of unbound, nontransferring Chl *a* in the preparation.

Carotenoid–Chl *a* Transfer. As of yet, no information is available on the dynamics of the carotenoid light harvesting process in the PSI core. We have studied β -carotene to Chl *a* energy transfer by exciting β -carotene at 510 nm and upconverting the carotenoid fluorescence from the carotenoid S_2 state at 580 nm and the Chl *a* fluorescence at 704 and 715 nm. Figure 7A shows the time-resolved fluorescence from the S_2 state of β -carotene at 580 nm. A single exponential fit indicates a lifetime of 105 fs. This lifetime closely corresponds to that recently determined for carotenoids bound to LHCI of plants by means of the fluorescence upconversion technique¹⁹ and is almost twice as long as that obtained for rhodopin glucoside in the LH2 complex of the purple photosynthetic bacterium *Rhodospirillum rubrum*.¹⁷ The S_2 state of β -carotene in

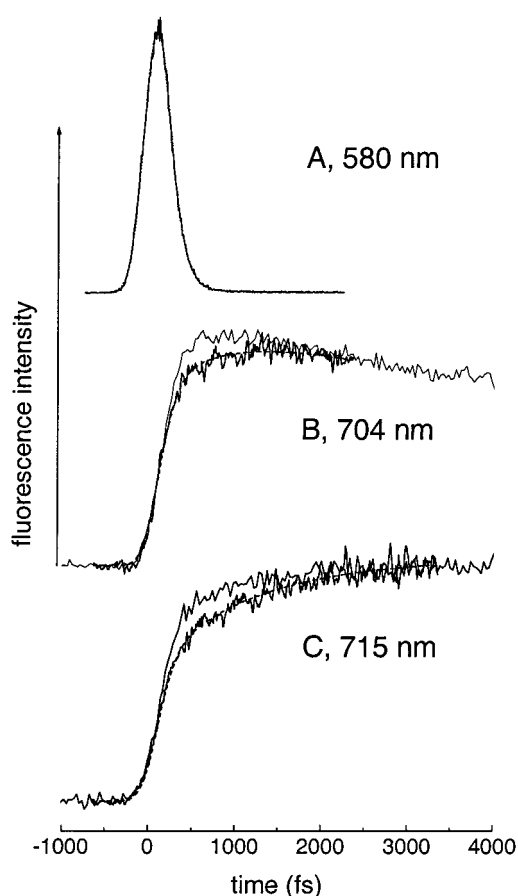


Figure 7. (A) Time-resolved fluorescence in *Synechococcus* PSI trimers upon excitation of β -carotene at 510 nm and detection at 580 nm. The trace is fitted with a single lifetime of 105 fs. (B) Thick solid line: time-resolved fluorescence upon excitation at 510 nm and detection at 704 nm. The dotted line denotes the results of a target analysis according to the kinetic scheme depicted in Figure 8; see text for details. Thin solid line: time-resolved fluorescence upon excitation of Chl *a* at 400 nm and detection at 704 nm. (C) Thick solid line: time-resolved fluorescence upon excitation at 510 nm and detection at 715 nm. Dotted line: result of the target analysis. Thin solid line: time-resolved fluorescence upon excitation of Chl *a* at 400 nm and detection at 715 nm.

solution has a solvent-dependent lifetime that ranges between 180 fs in nonpolar solvents and 120 fs in polar solvents.⁴⁵ The hydrophobic interior of the PSI core protein probably resembles a nonpolar solvent, which suggests that the “intrinsic” S_2 lifetime in PSI may be close to 180 fs. The observed lifetime of 105 fs in PSI is thus shortened, presumably as a result of energy transfer to Chl *a* from the S_2 state.

Figure 7B,C shows the upconverted fluorescence of Chl *a* at 704 and 715 nm (thick lines), respectively, upon excitation at 510 nm. For comparison, we also plotted the corresponding traces upon excitation at 400 nm (thin lines), which represent the dynamics of directly excited Chl *a*. The initial part of the fluorescence rises rapidly, which reflects the \sim 100 fs carotenoid–Chl transfer from the S_2 state. The signal subsequently rises further on a picosecond time scale. It is evident that the Chl *a* fluorescence at both 704 and 715 nm exhibits a slower rise component upon excitation of β -carotene as compared to Chl *a* Soret excitation. Our global analysis procedure of the data in Figures 4 and 5 indicated a rise component of 360 fs at 704 nm upon 400 nm excitation, which we attributed to equilibration among bulk Chl *a* molecules. A fit to the 510 nm excited trace at 704 nm (not shown) yields a distinctly slower rise component of 1.2 ps. This time constant probably originates

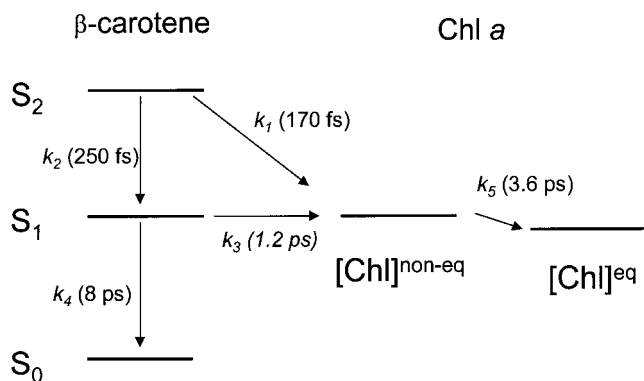


Figure 8. Kinetic scheme used for a target analysis of the data of Figure 7 to describe energy transfer pathways from β -carotene to Chl *a* in PSI trimers of *Synechococcus elongatus*. See text for details.

from carotenoid to Chl *a* energy transfer. The only candidate donor state would be the carotenoid S_1 state. However, such a direct assignment is precarious due to the convoluted Chl *a* energy transfer dynamics that follows energy transfer from the carotenoids.

To better characterize the S_1 -Chl *a* energy transfer process, we have conducted a so-called target analysis to our data,⁴⁶ in which we utilize our knowledge of Chl *a* dynamics to disentangle the energy transfer processes among Chls and between β -carotene and Chl *a*. We analyzed the three fluorescence-upconversion traces of Figure 7 in terms of the kinetic scheme depicted in Figure 8. In this minimal model, we assume that β -carotene transfers its energy uniformly to all spectral forms of Chl *a*, bulk and red pools alike, from both the S_2 state and the S_1 state. This results in a Chl *a* excited-state distribution after energy transfer from β -carotene identical to that upon nonselective Chl *a* excitation at 400 nm. Our analysis is based on the assumption that the time scales of energy transfer from the S_2 and S_1 states are clearly separated and lie in the order of 100 fs and 1 ps, respectively. In doing this, we may estimate the branching of excitations that reach Chl *a* through S_2 and S_1 by comparing the femtosecond and picosecond rise times in the signals at 705 and 716 nm, in which the picosecond part is affected by energy transfer among Chl *a* molecules. The model does not consider possible heterogeneities in the energy transfer characteristics of the 20 β -carotenes in the PSI core; it may of course well be that not all β -carotenes transfer their energy with equal efficiency, and with the fluorescence upconversion traces at 704 and 715 nm, evidently only those carotenoids are probed that do transfer their excitations to Chl *a*.

The energy transfer rate from the S_2 state to Chl *a*, k_1 , and internal conversion rate from S_2 to S_1 , k_2 , were chosen such to produce the observed S_2 lifetime of $1/(k_1 + k_2) = 105$ fs. The energy transfer rate constant from the S_1 state of β -carotene to Chl *a* is k_3 . We further assume that the intrinsic S_1 lifetime of β -carotene in the protein is the same as in solution and thus introduce decay into a loss channel at a rate $k_4 = (8 \text{ ps})^{-1}$.^{47,48} The fluorescence originating from the carotenoid S_2 state is assumed to be zero at the detection wavelengths 704 and 715 nm, and we assume that no fluorescence originates from the S_1 state. We take into account the internal Chl *a* dynamics by introducing two Chl compartments: one nonequilibrated bulk Chl *a*-C708/C719 compartment, denoted $[\text{Chl}]^{\text{non-eq}}$, which is populated from the S_1 and S_2 states of β -carotene, and one equilibrated bulk Chl *a*-C708/C719 compartment, denoted $[\text{Chl}]^{\text{eq}}$. The equilibration rate constant between bulk and red Chl *a*, k_5 , is fixed to $(3.6 \text{ ps})^{-1}$, as found above (see Figure 5). We did not include the 360 fs bulk Chl *a* equilibration

component in our model: our data are too sparse to justify such an increased complexity. An important requirement that we impose on the outcome of the model is that the fluorescence intensity amplitudes associated with the internal Chl *a* equilibration process are similar to those we determined in the SAS of Figure 5, in which $[\text{Chl}]^{\text{non-eq}}$ corresponds to the 3.6 ps SAS (solid circles) and $[\text{Chl}]^{\text{eq}}$ to the 9.6 ps SAS (triangles). Thus, when this analysis is performed, the adjustable parameters are the β -carotene S_1 -Chl *a* energy transfer rate constant k_3 and the relative rates of energy transfer from S_2 to Chl *a*, k_1 , and IC from S_2 to S_1 , k_2 .

We found that the most satisfactory result arises when the S_2 state of β -carotene branches into the S_1 state and Chl *a* at a ratio of 0.4:0.6. In the frame of our model, this would imply an internal conversion rate of $k_2 = (250 \text{ fs})^{-1}$ and an energy transfer rate $k_1 = (170 \text{ fs})^{-1}$. The rate constant for the S_1 -Chl *a* transfer process k_3 that results from the analysis is $(1.2 \text{ ps})^{-1}$. The resulting amplitude ratio of $[\text{Chl}]^{\text{non-eq}}:[\text{Chl}]^{\text{eq}}$ is 1.5:1 in the 704 nm trace and 0.7:1 in the 715 nm trace, in reasonable agreement with the SAS presented in Figure 5. The fitted curves are shown as the dotted lines in Figure 7. An S_1 -Chl *a* energy transfer rate constant of $(1.2 \text{ ps})^{-1}$ would imply an efficiency of 85% from the S_1 state. Taken into account the estimated 60% energy transfer efficiency from the S_2 state, this would lead to an overall carotenoid-Chl energy transfer efficiency of more than 90%, which is in line with the value found using fluorescence excitation measurements on *Synechocystis*.¹⁴ The resulting carotenoid-Chl *a* energy transfer rates in PSI are summarized in Figure 8.

The value of the S_2 - S_1 IC rate constant $k_2 = (250 \text{ fs})^{-1}$ that follows from our analysis is a point of concern. A rate of $(250 \text{ fs})^{-1}$ would lie significantly outside the range of aforementioned rates measured for β -carotene in the various solvents. However, if we fix k_2 to $(180 \text{ fs})^{-1}$ in the analysis, which is the IC rate reported for hexane, an S_2 lifetime of 105 fs implies a branching between the S_2 and S_1 pathways of 0.45:0.55, and this inevitably leads to an overestimation of the S_1 energy transfer pathway contribution to the picosecond part of the rise times in the 705 and 716 nm traces, which translates into unrealistic amplitudes for the 3.6 ps relaxation process of the two chlorophyll compartments. More precisely, in the 715 nm trace, $[\text{Chl}]^{\text{non-eq}}$ obtains a somewhat larger amplitude than $[\text{Chl}]^{\text{eq}}$, and in the 704 nm trace, the $[\text{Chl}]^{\text{non-eq}}$ amplitude becomes 3 times larger than that of $[\text{Chl}]^{\text{eq}}$, which is clearly at odds with the SAS shown in Figure 5. In principle, we cannot exclude that the S_2 to S_1 IC rate is slower in the protein than in nonpolar solvents. However, an equally sound explanation where we may maintain an IC rate close to $(180 \text{ fs})^{-1}$ is provided by asserting that a fraction of S_1 states may not or very poorly transfer its energy to Chl *a*. Given the lack of structural symmetry in PSI and the ensuing variety in pigment orientations and surroundings, this is not an unreasonable supposition. In this scenario, the relative contribution of the S_1 pathway could be lower than that of S_2 , consistent with our target analysis.

It is well established that the S_1 lifetime of β -carotene in solution is 8–10 ps and basically solvent-independent.^{47,48} We thus propose that this lifetime is shortened to 1.2 ps in at least a significant fraction of the β -carotene molecules in the PSI core complex as a result of energy transfer to Chl *a*. The situation sketched for PSI (Figure 8) is similar to that recently determined for LHCII of plants^{19,21} and for LH2 of purple bacteria^{20,22} and emphasizes that energy transfer from both S_2 and S_1 is required for an efficient light harvesting function of carotenoids.

It is interesting to compare the β -carotene dynamics in PSI with those in the PSII core antenna proteins CP43 and CP47. These complexes, which each bind 2 β -carotene molecules as their only carotenoids, are weakly homologous to the inner part of the PSI core antenna⁴⁹ and share structural similarities with it.⁵⁰ In CP43 and CP47, the energy transfer efficiency to Chl *a* is 35%,^{48,51} which is dramatically lower as compared to the PSI core complex. The S_1 lifetime of β -carotene in CP43 and CP47 is essentially the same as in solution, indicating that no or very little energy transfer occurs from the S_1 state.⁴⁸ This illustrates the very different roles that carotenoids may have in light harvesting systems that function under vastly different circumstances: PSI is an efficient and robust energy converter relatively insensitive to photodamage, and β -carotene strongly partakes in the overall goal of collecting as much light as possible. In contrast, the PSII core is a highly regulated light-harvesting system designed to carefully balance energy conversion and minimizing the photodamage that this process unavoidably accompanies; with relatively long Chl *a* lifetimes in the antenna, it has a relatively high probability of intersystem crossing to the Chl *a* triplet state, which along with the presence of an oxygen evolving complex gives rise to high concentrations of singlet oxygen. Under these perilous circumstances, β -carotene exerts an indispensable protective role by quenching Chl *a* triplets and especially singlet oxygen, and its light-harvesting purpose may be minute or even undesirable.

Let us consider the possible physical basis for the differences in energy transfer characteristics of β -carotene in PSI and PSII. Energy transfer from the S_2 state of β -carotene to Chl *a* in PSI and PSII probably proceeds at similar rates in the order of 100–200 fs, which appears to be a rather universal phenomenon in carotenoid-binding light harvesting antennae^{18,19,21,22} and may be understood from the concept of Förster-like energy transfer between molecules having strongly allowed optical transitions. The main difference in overall energy transfer efficiency between PSI and PSII cores lies in energy transfer from the S_1 state, which accounts for ~40% of the total carotenoid energy transfer in PSI and is basically nonexistent in PSII.

Generally, the energy transfer rate between a donor and acceptor molecule is proportional to the product of the spectral overlap and the square of the electronic coupling. The 0–0 energy level of the S_1 state of β -carotene in solution has been estimated to lie between 14 650 cm^{-1} (682 nm) and 14 100 cm^{-1} (709 nm),^{52,53} which is close to the Q_y level of Chl *a*. Considering the large width of the S_1 transition generally found in carotenoids (~3000 cm^{-1} ^{18,19,22,52}) and that the Q_y levels of Chl *a* in PSI and PSII are at most a few hundreds cm^{-1} apart, it seems likely that the spectral overlap of the S_1 state of β -carotene and Chl *a* is similar in PSI and PSII. However, a definite conclusion regarding this issue must await a determination of the in vivo S_1 energy level in PSI and PSII, as has been done for the LH2 complex of purple photosynthetic bacteria and LHClI of plants.^{18,19}

We next consider the possibility that the electronic coupling of the β -carotene S_1 and Chl Q_y states may be significantly larger in PSI as compared to PSII. A possible reason for a larger electronic coupling could be the significantly higher pigment density in PSI with respect to PSII; the PSI and PSII cores have approximately equal sizes but bind 100 and 35 Chls, and 20 and 6 β -carotenes, respectively.^{1,54,55} This leads to shorter interpigment distances and higher coordination numbers of energy accepting Chl *a* molecules.

It has recently been estimated that, in the LH2 complex of purple bacteria, the electronic coupling between the S_1 state of

carotenoids and BChl lies in the order of 10's of cm^{-1} , which lead to energy transfer time scales of a few picoseconds.²⁰ It was concluded from quantum chemical calculations that the "pure" S_1 state of carotenoids requires mixing with the strongly allowed S_2 state to produce a Coulombic coupling of the magnitude necessary for picosecond energy transfer rates.^{22,56,57} Symmetry breaking elements, be it in the carotenoid itself, interaction with other pigments, or its protein surroundings, could be responsible for such a phenomenon. In this respect, it is interesting to note that β -carotene in CP47 experiences an unusual, highly symmetric, and nonpolar environment,⁵⁸ which may imply a highly forbidden S_1 state for β -carotene in PSII. However, recent time-dependent density functional theoretical calculations have indicated that, strictly speaking, the S_1 state of the carotenoid does not need to have a transition moment to efficiently couple to nearby (B)Chls and that the magnitude of the Coulombic coupling may depend more critically on the geometrical details of donor and acceptor than on the extent of planar distortions of the carotenoid backbone.⁵⁹

At present, it remains an open question as of what exactly causes the differences in light-harvesting efficiency of β -carotene in PSI and PSII, and it is evident that additional spectroscopic information, combined with high-resolution structural models of the PSI and PSII core complexes and sophisticated structure-based calculations, are required for a better understanding of the versatility of roles that β -carotene can adopt in the PSI and PSII core complexes.

Acknowledgment. J.T.M.K acknowledges Dr. Cherri Hsu for enlightening discussions. J.T.M.K. is grateful to the Human Frontier Science Program Organization (HFSP) for granting a long-term fellowship. This work was supported by the Director, Office of Science, of the U.S. Department of Energy, under Contract No. DE-AC03-76SF00098. The research at Vrije Universiteit is supported by the Netherlands Organization for Scientific Research (NWO) via the Foundation of Earth and Life Sciences (ALW).

References and Notes

- (1) Krauss, N.; Schubert, W.-D.; Klukas, O.; Fromme, P.; Witt, T.; Saenger, W. *Nat. Struct. Biol.* **1996**, *3*, 965–973.
- (2) Schubert, W. D.; Klukas, O.; Krauss, N.; Saenger, W.; Fromme, P.; Witt, H. T. *J. Mol. Biol.* **1997**, *272*, 741–769.
- (3) Gobets, B.; van Amerongen, H.; Monshouwer, R.; Kruij, J.; Rögner, M.; van Grondelle, R.; Dekker, J. P. *Biochim. Biophys. Acta* **1994**, *1188*, 75–85.
- (4) Rätsep, M.; Johnson, T. W.; Chitnis, P. R.; Small, G. J. *J. Phys. Chem B* **2000**, *104*, 836–847.
- (5) Soukoulis, V.; Savikhin, S.; Xu, W.; Chitnis, P. G.; Struve, W. S. *Biophys. J.* **1999**, *76*, 2711–2715.
- (6) Karapetyan, N. V.; Dorra, D.; Schweitzer, G.; Bezsmertnaya, I. N.; Holzwarth, A. R. *Biochemistry* **1997**, *36*, 13830–13837.
- (7) Holzwarth, A. R.; Schatz, G.; Brock, H.; Bittersmann, E. *Biophys. J.* **1993**, *64*, 1813–1826.
- (8) van Grondelle, R.; Dekker, J. P.; Gillbro, T.; Sundström, V. *Biochim. Biophys. Acta* **1994**, *1187*, 1–65.
- (9) Gobets, B.; van Stokkum, I. H. M.; Rögner, M.; Kruij, J.; Schlodder, E.; Karapetyan, N. V.; Dekker, J. P.; van Grondelle, R. To be published.
- (10) Trissl, H.-W. *Photosynth. Res.* **1993**, *35*, 247–263.
- (11) Rivadossi, A.; Zucchelli, G.; Garlaschi, F. M.; Jennings, R. C. *Photosynth. Res.* **1999**, *60*, 209–215.
- (12) Karapetyan, N. V.; Holzwarth, A. R.; Rögner, M. *FEBS Lett.* **1999**, *460*, 395–400.
- (13) MacColl, R. *J. Struct. Biol.* **1998**, *124*, 311–334.
- (14) van der Lee, J.; Bald, D.; Kwa, S. L. S.; van Grondelle, R.; Rögner, M.; Dekker, J. P. *Photosynth. Res.* **1993**, *35*, 311–321.
- (15) Frank, H. A.; Cogdell, R. J. *Photochem. Photobiol.* **1996**, *63*, 257–264.
- (16) Koyama, Y.; Kuki, M.; Andersson, P. O.; Gillbro, T. *Photochem. Photobiol.* **1996**, *63*, 243–256.

- (17) Krueger, B. P.; Scholes, G. D.; Jimenez, R.; Fleming, G. R. *J. Phys. Chem. B* **1998**, *102*, 2284–2292.
- (18) Krueger, B. P.; Yom, J.; Walla, P. J.; Fleming, G. R. *Chem. Phys. Lett.* **1999**, *310*, 57–64.
- (19) Walla, P. J.; Yom, J.; Krueger, B. P.; Fleming, G. R. *J. Phys. Chem. B* **2000**, *104*, 4799–4806.
- (20) Walla, P. J.; Linden, P. A.; Hsu, C. P.; Scholes, G. D.; Fleming, G. R. *Proc. Natl. Acad. Sci. U.S.A.* **2000**, *97*, 10808–10813.
- (21) Gradinaru, C. C.; van Stokkum, I. H. M.; Pascal, A. A.; van Grondelle, R.; van Amerongen, H. *J. Phys. Chem.* **2000**, *104*, 9330–9342.
- (22) Zhang, J. P.; Fujii, R.; Qian, P.; Inaba, T.; Mizoguchi, T.; Koyama, Y.; Onaka, K.; Watanabe, Y.; Nagae, H. *J. Phys. Chem. B* **2000**, *104*, 3683–3691.
- (23) Du, M.; Xie, X.; Jia, Y.; Mets, L.; Fleming, G. R. *Chem. Phys. Lett.* **1993**, *201*, 535–542.
- (24) Hastings, G.; Kleinherenbrink, F. A. M.; Lin, S.; McHugh, T. J.; Blankenship, R. E. *Biochemistry* **1994**, *33*, 3193.
- (25) White, N. T. H.; Beddard, G. S.; Thorne, J. R. G.; Feehan, T. M.; Keyes, T. E.; Heathcote, P. *J. Phys. Chem.* **1996**, *100*, 12086–12099.
- (26) Dimagno, L.; Chan, C.-K.; Jia, Y.; Lang, M. J.; Newman, J. R.; Mets, L.; Fleming, G. R.; Haselkorn, R. *Proc. Natl. Acad. Sci. U.S.A.* **1995**, *92*, 2715–2719.
- (27) Savikhin, S.; Xu, W.; Soukoulis, V.; Chitnis, P. R.; Struve, W. *Biophys. J.* **1999**, *76*, 3278–3288.
- (28) Savikhin, S.; Xu, W.; Chitnis, P. R.; Struve, W. S. *Biophys. J.* **2000**, *79*, 1573–1586.
- (29) Melkozernov, A. N.; Lin, S.; Blankenship, R. E. *Biochemistry* **2000**, *39*, 1489–1498.
- (30) Gobets, B.; van Stokkum, I. H. M.; van Mourik, F.; Rögner, M.; Kruij, J.; Dekker, J. P.; van Grondelle, R. In *Photosynthesis: Mechanisms and Effects*; Garab, G., Ed.; Kluwer Academic Publishing: Dordrecht, The Netherlands, 1998; pp 571–574.
- (31) Gobets, B.; Dekker, J. P.; van Grondelle, R. 1998 in *Photosynthesis: Mechanisms and Effects*; Garab, G., Ed.; Kluwer Academic Publishing: Dordrecht, The Netherlands, 1998; pp 503–508.
- (32) Pålsson, L. O.; Dekker, J. P.; Schlodder, E.; Monshouwer, R.; van Grondelle, R. *Photosynth. Res.* **1996**, *48*, 239–246.
- (33) Pålsson, L. O.; Flemming, C.; Gobets, B.; van Grondelle, R.; Dekker, J. P.; Schlodder, E. *Biophys. J.* **1998**, *74*, 2611–2622.
- (34) Fromme, P.; Witt, H. T. *Biochim. Biophys. Acta* **1998**, *1365*, 175–184.
- (35) Byrdin, M.; Rimke, I.; Schlodder, E.; Stehlik, D.; Roelofs, T. A. *Biophys. J.* **2000**, *79*, 992–1007.
- (36) van Stokkum, I. H. M.; Beekman, L. M. P.; Jones, M. R.; van Brederode, M. E.; van Grondelle, R. *Biochemistry* **1997**, *36*, 11360–11368.
- (37) Cross, A. J.; Fleming, G. R. *Biophys. J.* **1984**, *46*, 45–56.
- (38) Donovan, B.; Walker, L. A., II; Yocum, C.; Sension, R. J. *J. Phys. Chem.* **1996**, *100*, 1945–1949.
- (39) Bradforth, S. E.; Jimenez, R.; van Mourik, F.; van Grondelle, R.; Fleming, G. R. *J. Phys. Chem.* **1995**, *99*, 16179–16191.
- (40) Jimenez, R. R.; Dikshit, S. N.; Bradforth, S. E.; Fleming, G. R. *J. Phys. Chem.* **1996**, *100*, 6825–6834.
- (41) Pullerits, T.; Chachisvilis, M.; Sundström, V. *J. Phys. Chem.* **1996**, *100*, 10787–10792.
- (42) Kennis, J. T. M.; Streltsov, A. M.; Vulto, S. I. E.; Aartsma, T. J.; Nozawa, T.; Amesz, J. *J. Phys. Chem. B* **1997**, *101*, 7827–7834.
- (43) Savikhin, S.; Struve, W. S. *Biochemistry* **1994**, *33*, 11200–11208.
- (44) Vulto, S. I. E.; Streltsov, A. M.; Aartsma, T. J. *J. Phys. Chem. B* **1997**, *101*, 4845–4850.
- (45) MacPherson, A. N.; Gillbro, T. *J. Phys. Chem. A* **1998**, *102*, 5049–5058.
- (46) Holzwarth, A. R. In *Biophysical Techniques in Photosynthesis*; Amesz, J., Hoff, A. J., Eds.; Kluwer: Dordrecht, The Netherlands, 1996; pp 75–92.
- (47) Wasielewski, M. R.; Johnson, D. G.; Bradford, E. G.; Kispert, L. D. *J. Chem. Phys.* **1989**, *91*, 6691–6697.
- (48) de Weerd, F.; van Grondelle, R. Manuscript in preparation.
- (49) Fromme, P.; Witt, H. T.; Schubert, W. D.; Klukas, O.; Saenger, W.; Krauss, N. *Biochim. Biophys. Acta* **1996**, *1275*, 76–83.
- (50) Rhee, K.-H.; Morris, E. P.; Barber, J.; Kuhlbrandt, W. *Nature* **1998**, *396*, 283–286.
- (51) van Dorssen, R. J.; Breton, J.; Plijter, J. J.; Satoh, K.; van Gorkom, H. J.; Amesz, J. *Biochim. Biophys. Acta* **1987**, *893*, 267–274.
- (52) Onaka, K.; Fuji, R.; Nagae, H.; Kuki, M.; Koyama, Y.; Watanabe, Y. *Chem. Phys. Lett.* **1999**, *315*, 75–81.
- (53) Chynwat, V.; Frank, H. A. *Chem. Phys.* **1995**, *194*, 237–244.
- (54) Boekema, E. J.; Boonstra, A. F.; Dekker, J. P.; Rögner, M. J. *Bioenerg. Biomembr.* **1994**, *26*, 17–29.
- (55) van Leeuwen, P. J.; Nieveen, M. C.; van der Meent, E. J.; Dekker, J. P.; van Gorkom, H. J. *Photosynth. Res.* **1991**, *28*, 149–153.
- (56) Nagae, H.; Kakitani, T.; Katoh, T.; Mimuro, M. *J. Chem. Phys.* **1993**, *98*, 8012–8023.
- (57) Damjanovic, A.; Ritz, T.; Schulten, K. *Phys. Rev. E* **1999**, *59*, 3293–3311.
- (58) Renge, I.; van Grondelle, R.; Dekker, J. P. *J. Photochem. Photobiol., A* **1996**, *96*, 109–121.
- (59) Hsu, C. P.; Walla, P. J.; Fleming, G. R.; Head-Gordon, M. Manuscript in preparation.